AIMS Materials Science, 4(6): 1202-1219.
DOI: 10.3934/matersci.2017.6.1202
Received: 22 September 2017
Accepted: 16 November 2017
Published: 21 November 2017

http://www.aimspress.com/journal/Materials

Research article

Stress field of a near-surface basal screw dislocation in elastically anisotropic hexagonal crystals

Valeri S. Harutyunyan [1,*], Ashot P. Aivazyan [1], and Andrey N. Avagyan [2]

[1] Department of Solid State Physics, Yerevan State University, 0025 Yerevan, Armenia
[2] Almaz Synthesis LTD, 0069 Yerevan, Armenia

* **Correspondence:** Email: vharut@ysu.am.

Abstract: In this study, we derive and analyze the analytical expressions for stress components of the dislocation elastic field induced by a near-surface basal screw dislocation in a semi-infinite elastically anisotropic material with hexagonal crystal lattice. The variation of above stress components depending on "free surface–dislocation" distance (i.e., free surface effect) is studied by means of plotting the stress distribution maps for elastically anisotropic crystals of GaN and TiB_2 that exhibit different degrees of elastic anisotropy. The dependence both of the image force on a screw dislocation and the force of interaction between two neighboring basal screw dislocations on the "free surface–dislocation" distance is analyzed as well. The influence of elastic anisotropy on the latter force is numerically analyzed for GaN and TiB_2 and also for crystals of such highly elastically-anisotropic materials as Ti, Zn, Cd, and graphite.

The comparatively stronger effect of the elastic anisotropy on dislocation-induced stress distribution quantified for TiB_2 is attributed to the higher degree of elastic anisotropy of this compound in comparison to that of the GaN. For GaN and TiB_2, the dislocation stress distribution maps are highly influenced by the free surface effect at "free surface–dislocation" distances roughly smaller than ≈15 and ≈50 nm, respectively. It is found that, for above indicated materials, the relative decrease of the force of interaction between near-surface screw dislocations due to free surface effect is in the order Ti > GaN > TiB_2 > Zn > Cd > Graphite that results from increase of the specific shear anisotropy parameter in the reverse order Ti < GaN < TiB_2 < Zn < Cd < Graphite. The results obtained in this study are also applicable to the case when a screw dislocation is situated in the "thin film–substrate" system at a (0001) basal interface between the film and substrate provided that the elastic constants of the film and substrate are the same or sufficiently close to each other.

Keywords: elastic anisotropy; screw dislocation; stress field; stress distribution map; free surface

effect; gallium nitride; titanium diboride; graphite

1. Introduction

The dislocation strain/stress field substantially affects mechanical, optical, electrical, and other physical properties of bulk materials and their thin films [1,2,3]. Therefore, the theoretical investigations of the dislocation stress field are of practical importance and enable to quantify the influence of dislocations on structure-property relationships. The character of the stress distribution produced by an individual dislocation in a crystalline material strongly depends on the type of dislocation (screw, edge or mixed), elastic properties of the material (elastic constants), and relative location of the dislocation with respect to free surface(s) [1]. Regardless of the type of dislocation and elastic properties of the material, the dislocation elastic field drastically changes with approach of the dislocation position to a free surface [1,4]. This necessitates, in the calculations of the stress field of a near-surface dislocation, a proper account of the interaction of dislocation with the free surface.

The influence of a free surface on the dislocation elastic field and the Peierls stress have been analyzed within the frameworks of the theory of isotropic elasticity in a large number of publications: particularly in studies [1,4–8] and other investigations.

For materials with pronounced elastic anisotropy, the elastic anisotropy was taken into account in theoretical studies of the dislocation stress field and other elastic characteristics for dislocation location in an infinite medium [9–14], close to interfacial surface in bicrystals [15–19], and at near-surface positions [10,18,19,20]. The elastic field for near-surface dislocation positions was theoretically studied for different types of the crystal lattice: cubic, trigonal, hexagonal, and other types [1,10,11,12,14,15,17–21].

However, the review of the results reported in above cited references and other similar studies in literature show that, for hexagonal crystals with considerable elasticity anisotropy, the theoretical investigations of the stress field produced by near-surface individual basal dislocations have received a little attention. A broad variety of elastically anisotropic compounds with hexagonal crystal lattice (BN, AlN, GaN, InN, SiC, TiB_2, graphite, etc.) has extensive applications in production of optical, semiconductor, microelectronic, and other type devices [2,22,23]. Production of these devices is mostly accompanied by formation of unavoidable dislocations that are located at hetero-interfaces (misfit dislocations) and/or in the vicinity of a free surface (near-surface dislocations). It is of particular interest to study the peculiarities of the stress field of near-surface basal dislocations in the case when the free surface by itself is a (0001) basal plane. In the technologies of heteroepitaxial deposition of semiconductor thin films with hexagonal crystal lattice, a frequently used deposition surface both for epitaxial films and substrates is the (0001) basal surface [2,22,24]. Especially for materials with pronounced elastic anisotropy, the above specified investigations will be helpful for precise quantification of the dislocation energy and interaction of the dislocation with neighboring near-surface defects (other individual dislocations, dislocation arrays, and point defects) and the (0001) free surface. It is also of interest to quantify and compare the effect of the elastic anisotropy on dislocation stress field for materials with hexagonal crystal lattice exhibiting different degrees of elastic anisotropy. In above comparative analysis, it may be helpful to use the so-called elasticity anisotropy parameters that are in detail analyzed in studies [25,26,27] and quantified for group

III-nitrides in our earlier work [28].

In this study, on the basis of the Chou's theoretical results [11,12], we derive and analyze the analytical expressions for stress components of the dislocation elastic field induced by a near-surface basal screw dislocation in a semi-infinite elastically anisotropic material with hexagonal crystal lattice. The variation of above stress components depending on "free surface–dislocation" distance (i.e., free surface effect) is studied by means of plotting the stress distribution maps for elastically anisotropic crystals of GaN (gallium nitride) and TiB_2 (titanium diboride) that exhibit different degrees of elastic anisotropy. The dependence both of the image force on a screw dislocation and the force of interaction between two neighboring basal screw dislocations on the "free surface–dislocation" distance is analyzed as well. The influence of elastic anisotropy on the latter force is numerically analyzed for GaN and TiB_2 and also for crystals of such highly elastically-anisotropic materials as Ti, Zn, Cd, and graphite.

2. Statement of the Problem

Our theoretical study is restricted to the following conditions:

(i) a basal-plane perfect screw dislocation is situated near a free surface of an elastically anisotropic bulk single crystal with hexagonal crystal lattice,

(ii) the dislocation line that is directed along the $<11\bar{2}0>$ crystallographic direction is parallel to the free surface, which coincides with a (0001) basal plane,

(iii) in terms of dislocation near-surface position (or extension of the dislocation elastic field), the crystal is considered as a semi-infinite medium.

The main aim of this study is presented at the end of Section 1. It should be clarified that, among the materials of interest in this study, the GaN may crystallize both in the zinc blende and wurtzite crystal structure with cubic and hexagonal crystal lattice, respectively [29], so for GaN the present study relates to the latter type of the crystal lattice.

3. Stress Components of a Near-surface Screw Dislocation

According to Section 2, Figure 1 schematically shows a basal-plane perfect screw dislocation (solid circle) in a semi-infinite single crystal, with dislocation line situated at a distance *h* from the free (0001) surface. The dislocation line that coincides with $<11\bar{2}0>$ direction is perpendicular to the plane of figure. We introduce a right-handed Cartesian coordinate system *xyz* with the *z* axis directed along the dislocation line and *y* axis oriented normal to the free surface (this means that the *z* and *y* axes are parallel to $<11\bar{2}0>$ and [0001] crystallographic directions, respectively). The Burgers vector of this dislocation, $a/3<11\bar{2}0>$, is directed along the *z* axis (*a* is the lattice constant in the basal plane). The magnitude of the Burgers vector b_s is equal to above specified lattice constant, $b_s = a$ [1]. It is assumed that the dislocation is also right-handed. In elastically anisotropic infinite medium with hexagonal crystal lattice, the non-zero stress components of the elastic field induced by above specified basal screw dislocation are given as [11,12]:

$$\sigma_{zx}^{(\mathrm{inf})} = -\frac{K_s b_s}{2\pi}\frac{\gamma y}{x^2+\gamma y^2}, \tag{1}$$

$$\sigma_{zy}^{(\mathrm{inf})} = \frac{K_s b_s}{2\pi} \frac{x}{x^2 + \gamma y^2}, \tag{2}$$

where

$$K_s = [0.5(c_{11} - c_{12})\, c_{44}]^{1/2}, \tag{3}$$

$$\gamma = \frac{0.5(c_{11} - c_{12})}{c_{44}}. \tag{4}$$

In Eqs. (1)–(4), b_s is the magnitude of the Burgers vector, K_s is the dislocation energy factor, and c_{ij} are the elastic stiffness constants of the crystal. Note that both stress components given by Eqs. (1) and (2) are of shear type. According to a known approach [1], in order to take into account the influence of the free surface on above stress components, it is necessary to introduce an image screw dislocation, with the opposite Burgers vector, at the same distance *h* from the free surface (in Figure 1, the image dislocation is shown by an empty circle). In the defined coordinate system *xyz* (see Figure 1), the dislocation lines of the real and image dislocations are situated at positions $(x = 0, y = 0)$ and $(x = 0, y = 2h)$, respectively. By a replacement $y \to (y - 2h)$ in Eqs. (1) and (2) and changing the signs of both stress components into opposite ones, we obtain the stress components of the image dislocation in infinite medium:

$$\sigma_{zx}^{(im)} = \frac{K_s b_s}{2\pi} \frac{\gamma (y - 2h)}{x^2 + \gamma (y - 2h)^2}, \tag{5}$$

$$\sigma_{zy}^{(im)} = -\frac{K_s b_s}{2\pi} \frac{x}{x^2 + \gamma (y - 2h)^2}. \tag{6}$$

Finally, the shear stress components of a real screw dislocation at a distance *h* from the free surface, σ_{zx} and σ_{zy}, are determined as a superposition of the corresponding stress components given by Eqs. (1), (2), (5), and (6):

$$\sigma_{zx} = \sigma_{zx}^{(\mathrm{inf})} + \sigma_{zx}^{(im)} = -\frac{K_s b_s}{2\pi} \left[\frac{\gamma y}{x^2 + \gamma y^2} - \frac{\gamma (y - 2h)}{x^2 + \gamma (y - 2h)^2} \right], \tag{7}$$

$$\sigma_{zy} = \sigma_{zy}^{(\mathrm{inf})} + \sigma_{zy}^{(im)} = \frac{K_s b_s}{2\pi} \left[\frac{x}{x^2 + \gamma y^2} - \frac{x}{x^2 + \gamma (y - 2h)^2} \right], \tag{8}$$

where parameters K_s and γ given by Eqs. (3) and (4) take into account the elasticity anisotropy of the crystal. From Eq. (8), it follows that the necessary boundary condition $\sigma_{zy}(y = h) = 0$ at the free surface is fulfilled.

Owing to replacements $K_s \to G$ and $\gamma \to 1$ [11,12], Eqs. (7) and (8) reduce to known expressions for dislocation stress components in the case of an elastically isotropic medium [1]:

$$\sigma_{zx} = -\frac{Gb_s}{2\pi}\left[\frac{y}{x^2+y^2} - \frac{y-2h}{x^2+(y-2h)^2}\right], \tag{9}$$

$$\sigma_{zy} = \frac{Gb_s}{2\pi}\left[\frac{x}{x^2+y^2} - \frac{x}{x^2+(y-2h)^2}\right], \tag{10}$$

where G is the isotropic shear modulus.

Eqs. (1), (2), and (5)−(10) are applicable in the spatial region out of the dislocation core. In the first approximation, the radius of the dislocation core is estimated to be $\approx b_s$ [1].

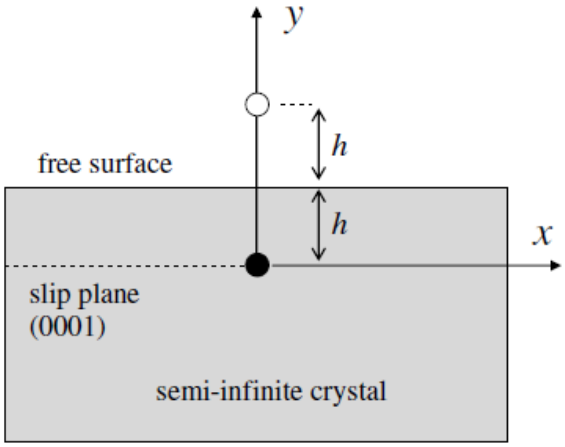

Figure 1. Positions of a near-surface basal screw dislocation (solid circle) and image dislocation (empty circle) with respect to the free surface of a semi-infinite crystal. The real and image dislocations are situated at positions $(x=0, y=0)$ and $(x=0, y=2h)$, respectively. Both the free surface and the dislocation slip plane are (0001) basal planes.

4. Quantification of the Effect of Elastic Anisotropy on Dislocation Stress Field

In order to quantify solely the effect of elastic anisotropy on dislocation stress field, we consider the dislocation stress distribution in an infinite medium, since in this case the stress distribution is not influenced by a free surface. We numerically compare for σ_{zx} component the spatial stress distribution with account of elastic anisotropy [Eq. (1) in combination with Eqs. (3) and (4)] with that in the approximation of elastic isotropy. In the approximation of elastic isotropy, the σ_{zx} stress component is achieved from Eq. (1) owing to above specified replacements $K_S \to G$ and $\eta \to 1$:

$$\sigma_{zx} = -\frac{Gb_s}{2\pi}\frac{y}{x^2+y^2} \quad . \tag{11}$$

In Eq. (11), as in Eqs. (9) and (10), G is the isotropic shear modulus. The above comparative analysis is conducted for two materials, GaN and TiB_2, that exhibit mutually different degrees of elastic anisotropy (see Section 8). For a basal screw dislocation in an infinitely large GaN crystal, Figure 2a shows the plots for dependences $\sigma_{zx}(x)$ according to Eqs. (1) and (11) in the case of

application of anisotropic and isotropic elasticity theory, respectively. The above $\sigma_{zx}(x)$ dependences are presented for (*x*,*y*) points that lie on the lines $y = 0.15x$, $y = 0.3x$, and $y = x$ in the range of $2b_s < x < 100$ Å [note that the above lines cross the dislocation position $(x = 0, y = 0)$]. Analogously with the case of GaN, Figure 2b shows for an infinitely large TiB_2 crystal the plots of dependences $\sigma_{zx}(x)$ in the range of $2b_s < x < 100$ Å according to Eqs. (1) and (11) along the radial directions $y = 0.3x$, $y = x$, and $y = 5x$. In the plots presented in Figure 2, for the sake of convenience the sign minus in Eqs. (1) and (11) was omitted and the following parametric data have been used: for GaN and TiB_2, $b_s = a = 3.19$ Å [29] and $b_s = a = 3.03$ Å [30], respectively, and the data for stiffness constants c_{ij} [31,32] and shear modulus G from Table 1 and Table 2, respectively. It should be detailed that the isotropic shear modulus G in Eq. (11) we defined as the Voigt-Reuss-Hill shear modulus, G_{VRH}, that is achieved from expression [33]

$$G \equiv G_{VRH} = \frac{G_R + G_V}{2}, \tag{12}$$

where G_R and G_V are the isotropic lower and upper limits of the shear modulus resultant from the Reuss and Voigt averaging schemes, respectively. Along with the data for modulus G, Table 2 also lists the calculated data for moduli G_R and G_V that are achieved with the use of c_{ij} stiffness constants presented in Table 1. For the sake of brevity, we omit here the details of these calculations that may be found particularly in study [34]. The data for the dislocation energy factor K_s and parameter γ, calculated according to Eqs. (3) and (4) with the use of c_{ij} values from Table 1, are presented in Table 2 as well.

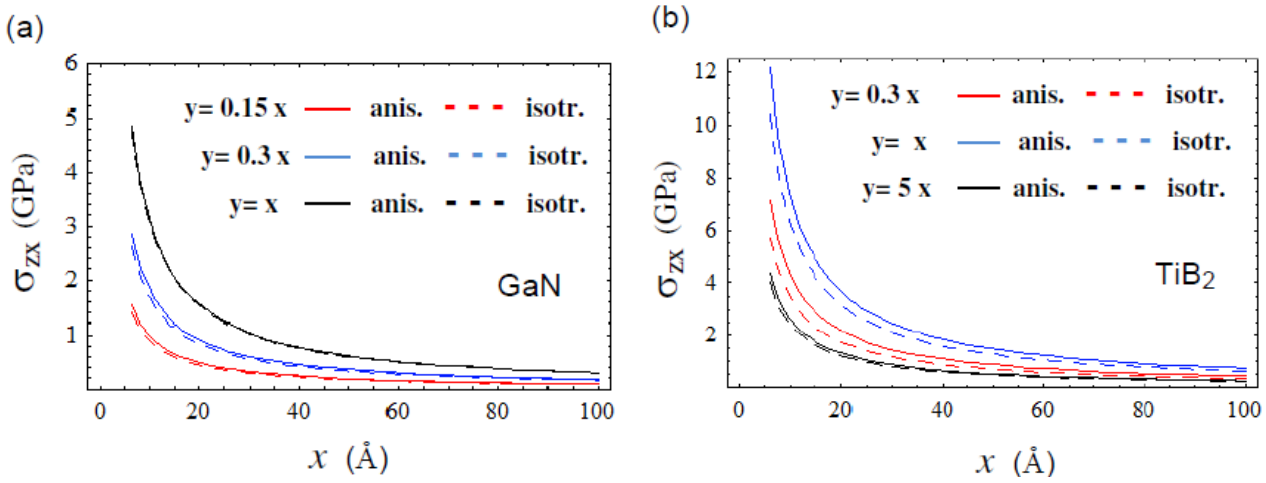

Figure 2. (a) Dependences $\sigma_{zx}(x)$ for a basal screw dislocation in an infinitely large GaN crystal along the radial directions $y = 0.15x$, $y = 0.3x$, and $y = x$. (b) Dependences $\sigma_{zx}(x)$ for a basal screw dislocation in an infinitely large TiB_2 crystal along the radial directions $y = 0.3x$, $y = x$, and $y = 5x$. In (a) and (b), solid lines are the plots within anisotropic elasticity theory according to Eq. (1), dashed lines are the plots in the approximation of isotropic elasticity theory according to Eq. (11).

Table 1. Elastic stiffness constants in GPa units.

Material	c_{11}	c_{12}	c_{44}	c_{13}	c_{33}	Ref.
GaN	390	145	105	106	398	[31]
TiB_2	660	48	260	93	432	[32]

Table 2. Energy factor K_S (Eq. (3)), isotropic shear moduli G_R, G_V, and G (Eq. (12)), shear anisotropy parameter A (Eq. (17)), and parameter γ (Eq. (4)).

Material	K_S (GPa)	G_R (GPa)	G_V (GPa)	G (GPa)	A (%)	γ
GaN	113	119	121	120	0.83	1.17
TiB_2	282	258	266	262	1.53	1.18

5. Effect of the "Free Surface–Dislocation" Distance on Dislocation Stress Field

5.1. Effect on σ_{zx} Stress Component

The plots presented in Figure 2 show that, in the whole, the account of the elastic anisotropy both for GaN and TiB_2 crystals results in a non-negligible contribution into the dislocation stress distribution quantified in the approximation of isotropic elasticity. The above contribution is appreciable along the lines $y = 0.15x$ and $y = 0.3x$ for GaN (Figure 2a) and is considerable along the lines $y = 0.3x$ and $y = x$ for TiB_2 (Figure 2b). Therefore, it is more realistic to analyze/quantify the effect of the "free surface–dislocation" distance on dislocation stress field within the scope of the anisotropic elasticity theory.

For the case of a basal screw dislocation situated at a distance h from the free surface of a GaN crystal (Figure 1), Figures 3a–d show the contours of equal stress (i.e., maps of the stress spatial distribution) for dislocation σ_{zx} stress component at different values of $h = \infty$, 150, 80, and 40 Å. These contours are plotted according to Eq. (7) combined with Eqs. (3) and (4). Note that, in the limit case of $h = \infty$ corresponding to Figure 3a (the dislocation is situated in infinite crystal), Eq. (7) transforms to Eq. (1). In order to trace the degree of influence of the distance h on above stress maps, it was sufficient, in all plots in Figures 3a–d, to be restricted with σ_{zx} values/contours −1, −1.5, and −4 GPa in the spatial range of $y > 0$ and with σ_{zx} values/contours 1, 1.5, and 4 GPa in the spatial range of $y < 0$. Similarly to the previous case, for the case of location of a basal screw dislocation in a semi-infinite crystal of TiB_2, Figures 3e–h show the σ_{zx} stress maps for the same stress values (as in the case with GaN crystal) at different locations of the dislocation from the free surface $h = \infty$, 500, 200, and 100 Å. At $h = \infty$, the stress map is plotted according to Eq. (1) and, at h = 500, 200, and 100 Å, the stress maps are plotted according to Eq. (7). In all stress maps presented in Figure 3, the solid circle centered at position $(x = 0, y = 0)$ schematically shows the region occupied by the dislocation core. In the plotting of these stress maps, we used the values of the Burgers vector specified in Section 4 and the data for c_{ij} stiffness constants listed in Table 1.

5.2. Effect on σ_{zy} Stress Component

For the case of a dislocation situated at a distance *h* from the free surface of a GaN crystal, Figures 4a–c show the contours of equal stress for dislocation σ_{zy} stress component at different values of *h* = ∞, 20, and 10 Å. These contours are plotted according to Eq. (8) combined with Eqs. (3) and (4). Note that, in the limit case of *h* = ∞ corresponding to Figure 4a (dislocation is situated in infinite crystal), Eq. (8) transforms to Eq. (2). In order to trace the degree of influence of the distance *h* on above stress maps, it was sufficient, in all plots in Figures 4a–c, to be restricted with σ_{zy} values/contours 1.5, 3, and 7 GPa in the spatial range of $x > 0$ and with σ_{zy} values/contours −1.5, −3, and −7 GPa in the spatial range of $x < 0$. Similarly to the previous case, for the case of location of a basal screw dislocation in a TiB_2 crystal, Figures 4d–f show the σ_{zy} stress maps for the same stress values (as in the case with GaN crystal) at different locations of the dislocation from the free surface *h* = ∞, 40, and 20 Å. At *h* = ∞, the stress map is plotted according to Eq. (2) and, at *h* = 40 and 20 Å, the stress maps are plotted according to Eq. (8). In all stress maps presented in Figure 4, the solid circle centered at position $(x = 0, y = 0)$ schematically shows the region occupied by the dislocation core. In the plotting of these stress maps, we used the values of the Burgers vector specified in Section 4 and the data for c_{ij} stiffness constants listed in Table 1.

6. Interaction of Dislocation with Free Surface

In the case under consideration (Figure 1), the interaction force of a real dislocation with the free surface is quantified via the interaction force exerted by the image dislocation on the real dislocation [1]. In our case, the absolute value of this force (per unit length of the dislocation line) is determined with use of Eq. (5) as follows:

$$F = b_s \left| \sigma_{zx}^{(im)}(x = 0, y = 0) \right| = \frac{K_s b_s^2}{4\pi} \frac{1}{h}, \tag{13}$$

where $\sigma_{zx}^{(im)}(x = 0, y = 0)$ is the stress produced by image dislocation at position occupied by the real dislocation, $(x = 0, y = 0)$ (see Figure 1). Not that, according to Eq. (6), at position of the real dislocation $(x = 0, y = 0)$ the $\sigma_{zy}^{(im)}$ stress component of the image dislocation is zero and, hence, no force component is produced by this stress component on real dislocation. As the force between unlike screw dislocations (i.e., between the real and image dislocations) is attractive, this means that the force *F* (Eq. (13)) is directed along the positive direction of the *y* axis (see Figure 1). From the physical standpoint, this is equivalent to a statement that the free surface attracts the near-surface dislocation. Figure 5 shows the plots for dependence $F(h)$ according to Eq. (13) for the cases when a near-surface screw dislocation is situated in semi-infinite crystals of GaN and TiB_2.

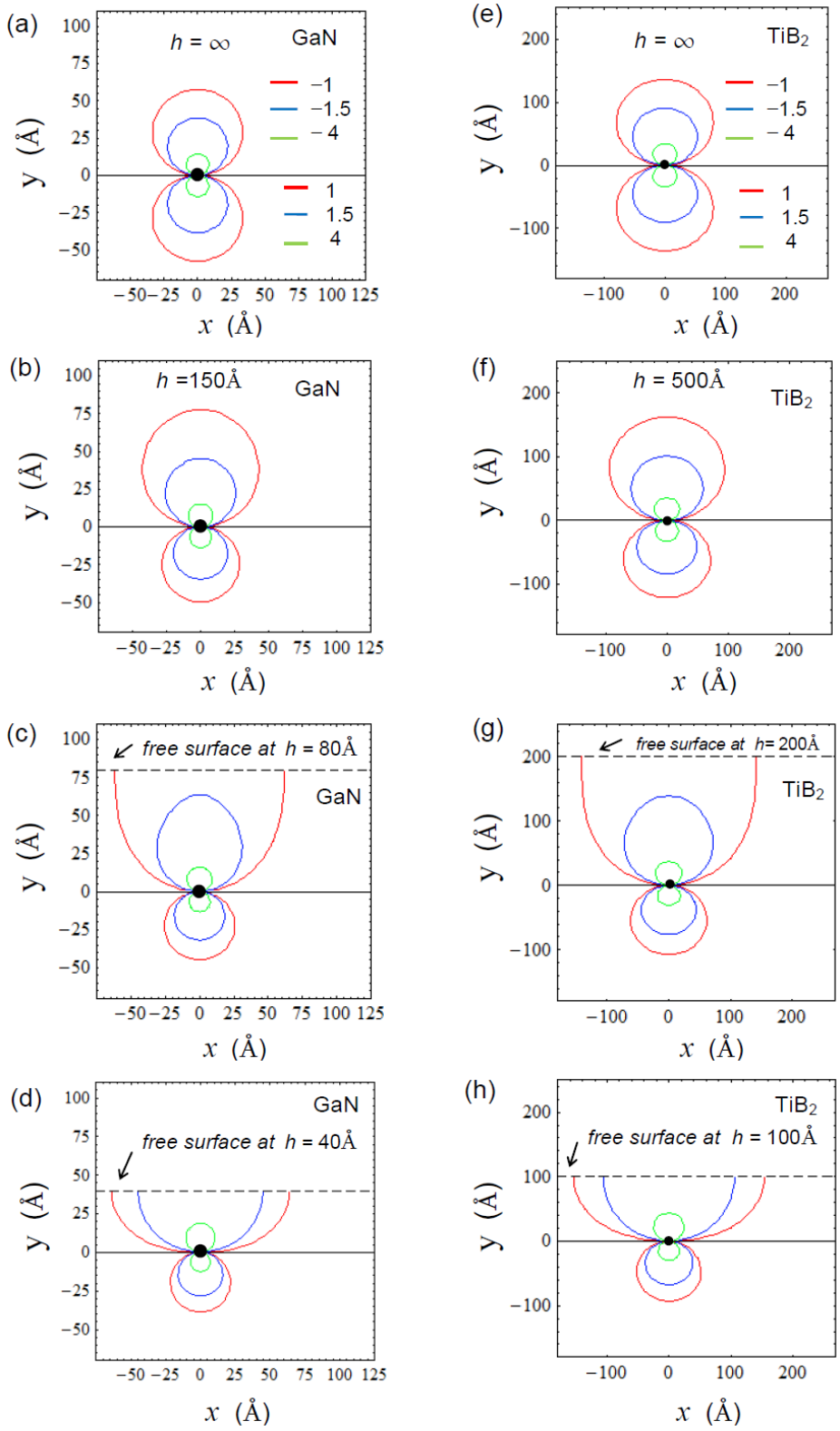

Figure 3. In GaN crystal, contours of equal stress for σ_{zx} stress component at different values of $h = \infty$ (a), 150 Å (b), 80 Å (c), and 40 Å (d). In TiB_2 crystal, contours of equal stress for σ_{zx} stress component at different values of $h = \infty$ (e), 500 Å (f), 200 Å (g), and 100 Å (h). In (a)–(h), the contours σ_{zx} = −1, −1.5, and −4 GPa are in the range of $y > 0$ and the contours σ_{zx} = 1, 1.5, and 4 GPa are in the range of $y < 0$.

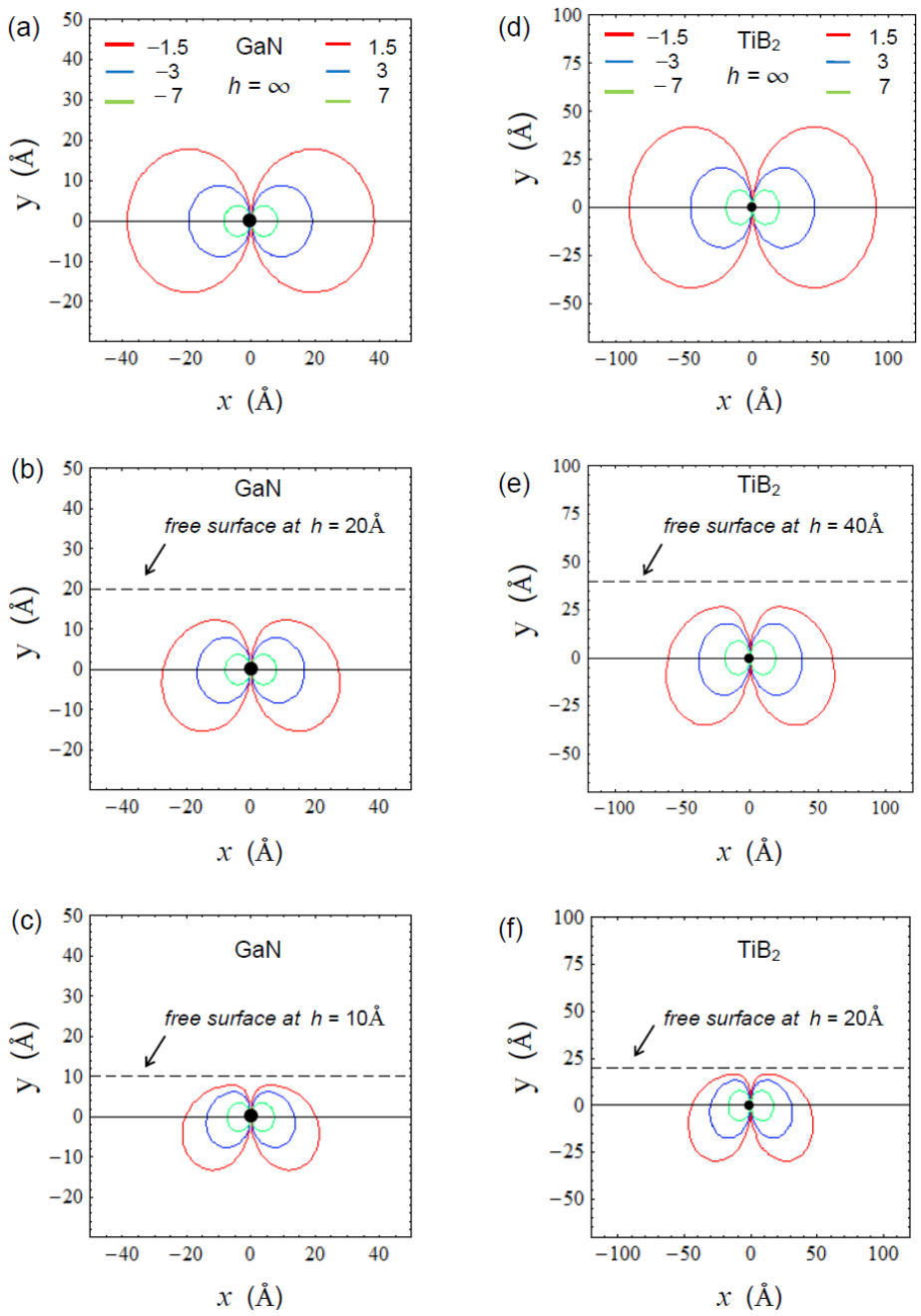

Figure 4. In GaN crystal, contours of equal stress for σ_{zy} stress component at different values of $h = \infty$ (a), 20 Å (b), and 10 Å (c). In TiB_2 crystal, contours of equal stress for σ_{zy} stress component at different values of $h = \infty$ (d), 40 Å (e), and 20 Å (f). In (a)–(f), the contours σ_{zx} = 1.5, 3, and 7 GPa are in the spatial range of $x > 0$ and the contours σ_{zx} = −1.5, −3, and −7 GPa are in the spatial range of $x < 0$.

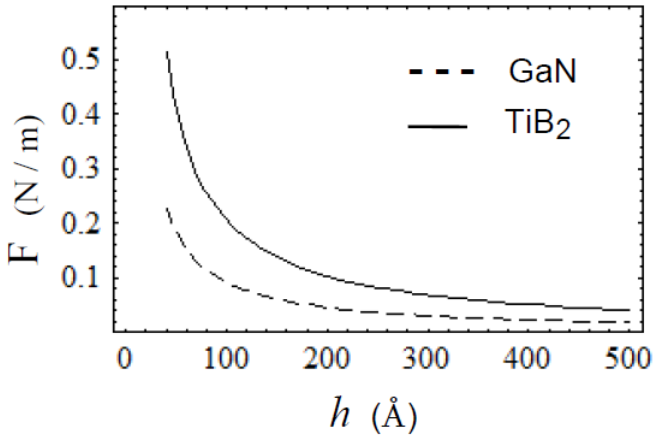

Figure 5. The dependence $F(h)$ according to Eq. (13) for the cases when a near-surface screw dislocation is situated in semi-infinite crystals of GaN and TiB_2.

7. Interaction of Two Neighboring Basal Screw Dislocations

In terms of dislocation slip in the (0001) basal plane, it is of particular interest interaction of two near-surface screw dislocations with parallel dislocations lines situated in the same basal plane. Figure 6a schematically shows these two dislocations and it is assumed that they have the same Burgers vector. In this case, the interaction force F exerted parallel to basal plane on each of these dislocations is repelling. This force may be determined with the use of Eq. (8) as the force exerted by the dislocation at position $(x = 0, y = 0)$ on the unit length of dislocation with position $(x = d,\ y = 0)$ (see Figure 6a):

$$F = b_s \sigma_{zy}(x = d,\, y = 0) = \frac{K_s b_s^2}{2\pi}\left[\frac{1}{d} - \frac{d}{d^2 + 4\gamma h^2}\right], \tag{14}$$

where d is the distance between dislocation lines. Figures 6b and 6c show the plots of the dependence $F(d)$ given by Eq. (14) at different values of parameter h for location of dislocations in TiB_2 and GaN crystals, respectively. It is helpful to represent Eq. (14) in the following equivalent form:

$$F = \frac{K_s b_s^2}{2\pi d}\left(1 - S_f\right), \tag{15}$$

where

$$S_f = \frac{1}{1 + 4\gamma\left(\frac{h}{d}\right)^2}. \tag{16}$$

The parameter S_f expressed through Eq. (16) is dependent on "free surface–dislocation" distance h and quantifies the effect/influence of free surface on interaction force. The following

obvious motivation allows to define the parameter S_f as the force-suppressing factor. According to Eq. (16), at a limited fixed interdislocation distance d, parameter S_f varies in the range $0 < S_f < 1$ with the lower and upper limits 0 and 1 that are achieved at limiting cases $h \to \infty$ (dislocations are positioned in an infinitely large crystal) and $h \to 0$ (position of dislocations tends to free surface), respectively. Accordingly, at above limits $h \to \infty$ (i.e., at $S_f \to 0$) and $h \to 0$ (i.e., at $S_f \to 1$), Eq. (15) results in upper and lower limits for the interaction force $F \to K_s b_s^2/(2\pi d)$ (no force suppression in infinitely large crystal) and $F \to 0$ (force is gradually suppressed with approach of dislocations to free surface), respectively. The above discussed trends associated with the suppression of the dislocation interaction force by a free surface are well reflected by the plots presented in Figures 6b and 6c. The degree of influence of parameter γ on parameters S_f and F [Eqs. (15) and (16)] is discussed in the next Section 8.

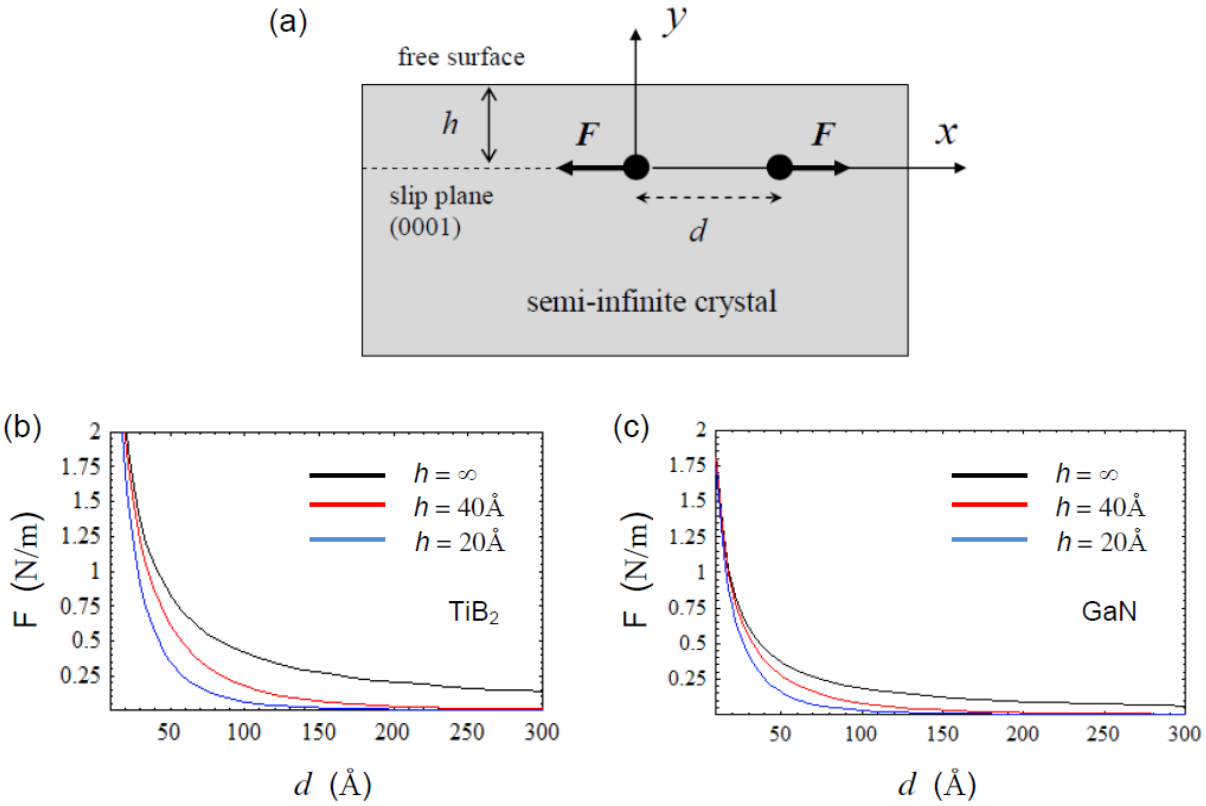

Figure 6. (a) Positions of two near-surface basal screw dislocations (solid circles) with respect to the free surface of a semi-infinite crystal. The dependences of the dislocation interaction force F on the distance d between dislocation lines (Eq. (14)) at different positions of dislocations from the free surface $h = \infty$, 40, and 20 Å for crystals of TiB_2 (b) and GaN (c).

8. Discussion

For analysis of the influence of elastic anisotropy on distribution of the dislocation stress field,

it is helpful for materials considered in this study to quantify the so-called elastic anisotropy parameter. There should be distinguished two types of elastic anisotropy for a material: compressive and shear anisotropy. The compressive anisotropy is associated with compressive deformation and quantifies the difference in the compressibility of the material in different crystallographic directions. The shear anisotropy is defined in analogous way but in terms of the shear deformation. Since this study deals with the screw type dislocation (both non-zero stress components of the dislocation stress field are of shear type), there is a sense to quantify for materials of interest, GaN and TiB_2, only the shear anisotropy parameter. The shear anisotropy parameter (expressed in per cent units) quantifies the degree of elastic anisotropy possessed by a crystal and is defined by the expression [25]

$$A = \frac{G_V - G_R}{G_V + G_R} 100\%, \tag{17}$$

where G_R and G_V are the isotropic shear moduli defined in Eq. (12). For GaN and TiB_2, the values of parameter A calculated according to Eq. (17) are presented in Table 2 and show that the degree of elastic anisotropy of a TiB_2 single crystal, $A = 1.53\%$, is about twice higher than that of a GaN single crystal, $A = 0.83\%$. It is worth noting that in the case of an elastically isotropic material $G_R = G_V$, and Eq. (17) results in $A = 0\%$ (i.e., no anisotropy in the elastic properties of the material at least in terms of the shear modulus). In the case of GaN, the numerical analysis of the plots presented in Figure 2a shows that, in comparison to the approximation of isotropic elasticity (Eq. (11)), the account of the elastic anisotropy (Eq. (1)) results in increase of the dislocation $\sigma_{zx}(x, y)$ stress component over (x, y) points of the dislocation stress field in average by $\approx 13\%$. In the case of TiB_2 (Figure 2b), this increase in the σ_{zx} stress component is in average on the level of $\approx 22\%$. The stronger effect of the elasticity anisotropy on dislocation-induced stress distribution in TiB_2 may be attributed to larger elastic anisotropy parameter of this compound, $A = 1.53\%$, in comparison to that of the GaN, $A = 0.83\%$.

As it follows from mathematical features of the stress distributions given by Eqs. (1) and (2) for a dislocation situated in an infinitely large crystal, both σ_{zx} and σ_{zy} stress contours should be symmetric in the shape with respect to both *x* and *y* coordinate axes (see Figures 3a and 4a for GaN and Figures 3e and 4d for TiB_2). At a finite distance *h* of a dislocation from the free surface, these contours preserve the spatial symmetry only with respect to the *y* axis (see Figures 3b–d and Figures 4b and 4c for GaN and Figures 3f–h and Figures 4e and 4f for TiB_2). Figures 3b–d (for the case of GaN) and Figures 3f–h (for the case of TiB_2) show that with approach of the dislocation position to the free surface (i.e., with decrease of the distance *h*) the σ_{zx} stress distribution in the dislocation elastic field drastically changes in the following way:

1) in the spatial range of $0 < y < h$, all contours expand in size; the lower stress contours split one after one into two separate parts with termination at the free surface [particularly, Figure 3d shows that at *h* = 40 Å the lowest (−1 GPa) and intermediate (−1.5 GPa) stress contours are split with termination at the free surface],

2) at the same time, in the spatial range of $y < 0$, all stress contours shrink towards the dislocation line/core position with no splitting.

Figures 4b and 4c (for the case of GaN) and Figures 4e and 4f (for the case of TiB_2) show that with approach of the dislocation position to a free surface (i.e., with decrease of the distance *h*) all σ_{zy} stress contours shrink towards the dislocation core position with no splitting. In comparison to

the case with a GaN crystal, in the case of a TiB_2 crystal both σ_{zx} and σ_{zy} stress contours are extended over wider spatial regions (see the stress maps in Figures 3 and 4) as a result of a comparatively larger value in the energy factor K_S in Eqs. (7) and (8) (see the data for K_S in Table 2).

The plots according to Eq. (13) (Figure 5) show that with approach of the dislocation to the free surface the image force (i.e., the force of interaction of dislocation with the free surface) monotonically increases. As it follows from Eq. (13), this force is larger in the case of a TiB_2 crystal compared to the case of a GaN crystal owing to a comparatively larger energy factor K_S in the former case.

The plots according to Eq. (14) (Figures 6b and 6c) show that with approach of a pair of dislocations to the free surface ($h \to 0$) the interaction force of dislocations, *F*, strongly decreases at all distances between dislocations, *d*. According to Eqs. (8) and (14), the above trend results from the following limit in the dependence $\sigma_{zy}(h)$ (Eq. (8)): $\sigma_{zy} \to 0$ when $h \to 0$. The plots presented in Figures 6b and 6c are interesting from the physical standpoint: at near-surface positions of dislocations, the force of interaction between dislocations experiences the "screening" effect of the free surface, i.e., the free surface partially suppresses this force. This force-suppressing effect is quantified by parameter S_f [see Eqs. (14)–(16)] discussed in Section 7. According to Eq. (16), the force-suppressing parameter S_f, except the geometrical parameters *d* and *h*, depends also on parameter γ. It should be noted that the parameter γ given by Eq. (4) is connected to the well-known Zener's shear anisotropy parameter, A_Z, via the relationship [25,27]

$$A_Z^{-1} = \gamma = \frac{G_p}{G_b}, \tag{18}$$

where, $G_p = 0.5(c_{11} - c_{12})$, $G_b = c_{44}$.

In Eq. (18) (or equivalently in Eq. (4)), G_p and G_b are understood as the prism plane and basal plane shear moduli, respectively. From Eq. (18), it follows that parameter γ is also valid for quantification of the shear anisotropy. However, it should be clarified that parameter A_Z (or parameter γ) is sufficient only for characterization of the degree of shear anisotropy in cubic crystal lattice. For characterization of the overall shear anisotropy in hexagonal crystal lattice, it is recommended [25] to use the parameter *A* (Eq. (17)), which takes into account the difference/anisotropy in the shear modulus on all possible crystallographic planes. Meanwhile, for hexagonal crystal lattice, the parameter γ characterizes the shear anisotropy only in terms of the shear moduli G_p and G_b defined in Eq. (18). In terms of the shear anisotropy parameter γ, (i) for an elastically isotropic material $G_p = G_b$ and Eq. (18) results in $\gamma = 1$ and (ii) for an elastically anisotropic material with $G_p < G_b$ or $G_p > G_b$, Eq. (18) results in $\gamma < 1$ or $\gamma > 1$, respectively. According to data in Table 2, the values of parameter γ for GaN and TiB_2 are very close: $\gamma = 1.17$ and 1.18, respectively. This means that, for these materials, the force-suppressing parameter S_f (Eq. (16)) is influenced by γ practically in the same degree. However, it is of interest to include into analysis of the dependence $S_f(\gamma)$ given by Eq. (16) also materials with the considerably higher shear anisotropy parameter γ than those of the GaN and TiB_2. Four such a type

materials with hexagonal crystal lattice, Ti, Zn, Cd, and graphite, are listed in Table 3 along with their stiffness constants and parameter γ calculated by Eq. (18). Note that, in terms of the anisotropy parameter γ, the graphite by of about two orders of magnitude is more anisotropic than both the GaN and TiB_2 with $\gamma \approx 1.2$. For quantitative analysis, Figure 7 presents the plot of the dependence $S_f(\gamma)$ (Eq. (16)) for a particular case when $d = h$ (this plot does not considerably change for $d > h$ or $d < h$ provided that the distances *d* and *h* are comparable). In this plot, the solid dots on the curve $S_f(\gamma)$ relate to GaN, TiB_2, and materials listed in Table 3. Parameter γ increases for these materials in the order Ti < GaN < TiB_2 < Zn < Cd < Graphite (see Tables 2 and 3) and this results in decrease of the force-suppressing parameter S_f in the reverse order Ti > GaN > TiB_2 > Zn > Cd > Graphite (Figure 7). The plot in Figure 7 shows that parameter S_f varies in a broad range, from ≈ 0.003 (for graphite) up to 0.25 (for Ti), and thereby demonstrates the importance of the account of elasticity anisotropy in the quantitative analysis of the interdislocation interaction forces. As an important conclusion, it should be noted that, in the case of graphite, parameter S_f is very small (≈ 0.003) and, according to Eq. (15), this results in a negligibly small effect of the free surface on the force of interaction between near-surface screw dislocations, *F*. This effect is somewhat enhanced (i.e., parameter S_f somewhat increases) under condition $d \gg h$ (see Eq. (16)). However, at large interdislocation distances *d*, the force *F* by itself drastically decreases (see Eq. (15)). From the physical standpoint, in graphite a very small effect of the (0001) free surface on the force of interaction between near-surface basal screw dislocations results from a weak bonding between crystallographic (0001) basal planes. Some important peculiarities of the dislocation-induced stress distribution in above considered highly anisotropic materials, Ti, Zn, Cd, and graphite, will be analyzed in our next study.

It is important to mention that, in the plots of stress maps of a near-surface screw dislocation, a very good agreement was achieved in the isotropic approximation between the results obtained particularly from Eq. (10) and corresponding atomistic simulation [18]. It would be also important the validation of analytical stress expressions for a near-surface screw dislocation in elastically anisotropic materials (Eqs. (7) and (8)) by atomistic simulation models.

The results obtained in this study are also applicable to the case when a screw dislocation is situated in the "thin film–substrate" system at a (0001) basal interface between the film and substrate provided that the elastic constants of the film and substrate are the same or sufficiently close to each other.

Table 3. Elastic stiffness constants in GPa units and shear anisotropy parameter γ.

Material	c_{11}	c_{12}	c_{44}	γ
Ti	162.4[a]	92.0[a]	46.7[a]	0.75
Zn	163.7[a]	36.4[a]	38.8[a]	1.64
Cd	113.8[a]	39.2[a]	20.0[a]	1.87
Graphite	1060[b]	180[b]	5[b]	88

[a] Ref. [35], [b] Ref. [36].

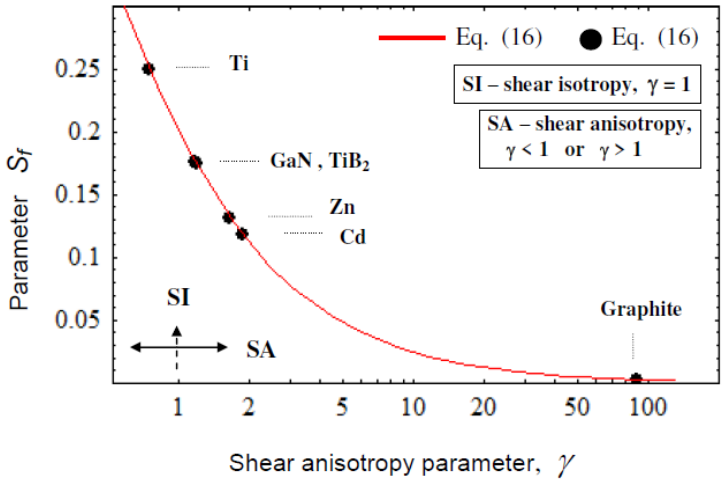

Figure 7. Dependence of the force-suppressing factor S_f on the shear anisotropy parameter γ according to Eq. (16) at $d = h$. The solid dots on the curve $S_f(\gamma)$ relate to GaN, TiB_2, and materials listed in Table 3.

9. Conclusion

Both the σ_{zx} and σ_{zy} dislocation stress components (Eqs. (7) and (8)) strongly depend on the position of dislocation with respect to a free surface.

For a dislocation positioned in an infinitely large crystal, both the σ_{zx} and σ_{zy} stress contours (Figures 3a and 3e and Figures 4a and 4d) are symmetric in shape with respect to both *x* and *y* coordinate axes. With approach of the dislocation position to the free surface, the above stress contours drastically change in shape (Figures 3b–d, 3f–h and Figures 4b, 4c, 4e, 4f) preserving the spatial symmetry only with respect to the *y* axis. In comparison to the case of a crystal with a smaller value of the dislocation energy factor (GaN), in a crystal with a larger value of this parameter (TiB_2) the stress contours are extended over wider spatial regions (Figures 3 and 4) and the interaction of a near-surface dislocation with the free surface (resultant from the σ_{zx} stress component) is stronger (Figure 5). For GaN and TiB_2, the dislocation stress distribution maps are highly influenced by the free surface effect at "free surface–dislocation" distances roughly smaller than ≈15 and ≈50 nm, respectively.

In terms of the shear anisotropy parameter *A* (Eq. (17)), the comparatively stronger effect of the elastic anisotropy on dislocation-induced stress distribution in TiB_2 is attributed to the higher degree of elastic anisotropy of this compound ($A = 1.53\%$) in comparison to that of the GaN ($A = 0.83\%$).

With approach of a pair of near-surface basal screw dislocations to (0001) free surface, their interaction force resultant from the σ_{zy} stress component strongly decreases at all interdislocation distances (Figure 6). With increase of the shear anisotropy parameter γ (Eq. (18)), the influence of free surface effect on above force decreases [Eqs. (15) and (16) and Figure 7]. For GaN and TiB_2 crystals, parameter γ is practically the same (≈ 1.2) and this results in about the same force-suppressing factor for these materials, $S_f \approx 0.175$ (Eq. (16) and Figure 7). Particularly for graphite, with a very large anisotropy parameter $\gamma (= 88)$, the force-suppressing factor, at

comparable distances *d* and *h* (Figure 6a), is negligibly small, $S_f \approx 0.003$ (Figure 7).

Conflict of Interest

All authors declare no conflict of interest in this paper.

References

1. Hirth JP, Lothe J (1982) *Theory of Dislocations*, New York: John Wiley & Sons.
2. Morkoc H (2008) *Handbook of Nitride Semiconductors and Devices*, Berlin: Wiley-VCH.
3. Telling RH, Heggie MI (2003) Stacking fault and dislocation glide on basal plane of graphite. *Phil Mag Lett* 83: 411–421.
4. Jagannadham K, Marcinkowski MJ (1978) Comparison of the image and surface dislocation models. *Phys Status Solidi A* 50: 293–302.
5. Cheng X, Shen Y, Zhang L, et al. (2012) Surface effect on the screw dislocation mobility over the Peierls barrier. *Phil Mag Lett* 92: 270–277.
6. Gars B, Markenscoff X (2012) The Peierls stress for coupled dislocation partials near a free surface. *Philos Mag* 92: 1390–1421.
7. Lee CL, Li S (2007) A half-space Peierls–Nabarro model and the mobility of screw dislocations in a thin film. *Acta Mater* 55: 2149–2157.
8. Liu L, Meng Z, Xu G, et al. (2017) Surface effects on the properties of screw dislocation in nanofilms. *Adv Mater Sci Eng* 2017.
9. Eshelby JD, Read WT, Shockley W (1953) Anisotropic elasticity with applications to dislocations theory. *Acta Metall* 1: 251–259.
10. Spence GB (1962) Theory of extended dislocations in symmetry directions in anisotropic infinite crystals and thin plates. *J Appl Phys* 33: 729–733.
11. Chou YT (1962) Interaction of parallel dislocations in a hexagonal crystal. *J Appl Phys* 33: 2747–2751.
12. Chou YT (1963) Characteristics of dislocation stress fields due to elastic anisotropy. *J Appl Phys* 34: 429–433.
13. Holec D (2008) Multi-Scale Modeling of III-Nitrides: from Dislocations to the Electronic Structure [PhD thesis]. University of Cambridge.
14. Chu HJ, Pan E, Wang J, et al. (2011) Three-dimensional elastic displacements induced by a dislocation of polygonal shape in anisotropic elastic crystals. *Int J Solids Struct* 48: 1164–1170.
15. Chu HJ, Wang J, Beyerlein IJ, et al. (2013) Dislocation models of interfacial shearing induced by an approaching glide dislocation. *Int J Plasticity* 41: 1–13.
16. Barnett DM, Lothe J (1974) An image force theorem for dislocations in anisotropic bicrystals. *J Phys F Metal Phys* 4: 1618–1635.
17. Wang J, Hoagland RG, Hirth JP, et al. (2008) Atomistic modeling of the interaction of glide dislocations with “weak” interfaces. *Acta Mater* 56: 5685–5693.
18. Wang L, Liu Z, Zhuang Z (2016) Developing micro-scale crystal plasticity model based on phase field theory for modeling dislocations in heteroepitaxial structures. *Int J Plasticity* 81: 267–283.
19. Chou YT (1966) On dislocation–boundary interaction in an anisotropic aggregate. *Phys Status Solidi B* 15: 123–127.

20. Chu H, Pan E (2014) Elastic fields due to dislocation arrays in anisotropic biomaterials. *Int J Solids Struct* 51: 1954–1961.
21. Shahsavari R, Chen L (2015) Screw dislocations in complex, low symmetry oxides: Core structures, energetics, and impact on crystal growth. *ACS Appl Mater Interfaces* 7: 2223–2234.
22. Ruterana P, Albrecht M, Neugebauer J (2003) *Nitride Semiconductors: Handbook on Materials and Devices*, Weinheim: Wiley-VCH Verlag GmbH & Co. KGaA.
23. Munro RG (2000) Material properties of titanium diboride. *J Res Natl Inst Stan* 105: 709–720.
24. Cheng TS, Davies A, Summerfield A, et al. (2016) High temperature MBE of graphene on sapphire and hexagonal boron nitride flakes on sapphire. *J Vac Sci Technol B* 34: 02L101.
25. Chung DH, Buessem WR (1968) The Elastic Anisotropy of Crystals, In: Vahldiek FW, Mersol SA, *Anisotropy in Single-Crystal Refractory Compounds*, New York: Plenum, 217–245.
26. Lethbridge ZAD, Walton RI, Marmier ASH, et al. (2010) Elastic anisotropy and extreme Poisson's ratios in single crystals. *Acta Mater* 58: 6444–6451.
27. Kube CM (2016) Elastic anisotropy of crystals. *AIP Adv* 6: 095209.
28. Specht P, Harutyunyan VS, Ho J, et al. (2004) Anisotropy of the elastic properties of wurtzite InN epitaxial films. *Defect Diff Forum* 226–228: 79–90.
29. Vurgaftman I, Meyer JR (2003) Band parameters for nitrogen-containing semiconductors. *J Appl Phys* 94: 3675–3696.
30. Wang HY, Xue FY, Zhao NH, et al. (2011) First-principles calculation of elastic properties of TiB_2 and ZrB_2. *Adv Mater Res* 150–151: 40–43.
31. Polian A, Grimsditch M, Grzegory I (1996) Elastic constants of gallium nitride. *J Appl Phys* 79: 3343–3344.
32. Spoor PS, Maynard JD, Pan MJ, et al. (1997) Elastic constants and crystal anisotropy of titanium diboride. *Appl Phys Lett* 70: 1959–1961.
33. Peselnick L, Meister R (1965) Variational method of determining effective moduli of polycrystals: (A) hexagonal symmetry, (B) trigonal symmetry. *J Appl Phys* 36: 2879–2884.
34. Watt JP, Peselnick L (1980) Clarification of the Hashin-Shtrikman bounds on the effective elastic moduli of polycrystals with hexagonal, trigonal, and tetragonal symmetries. *J Appl Phys* 51: 1525–1531.
35. Simmons G, Wang H (1971) *Single crystal elastic constants and calculated aggregate properties: a Handbook*, Cambridge, Massachusetts: The MIT Press.
36. Cousins CSG, Heggie MI (2003) Elasticity of carbon allotropes. III. Hexagonal graphite: Review of data, previous calculations, and a fit to a modified anharmonic Keating model. *Phys Rev B* 67: 024109.

AIMS Press